RESEARCH ARTICLE

Key Points:
- Simple, parsimonious ET schemes for integrated hydrological models are assessed
- Boundary condition switching is suitable only for shallow root depths
- Oxygen stress and root water compensation influence riparian zone ET dynamics

Correspondence to:
M. Camporese,
matteo.camporese@unipd.it

Catchment-scale Richards equation-based modeling of evapotranspiration via boundary condition switching and root water uptake schemes

Matteo Camporese[1], Edoardo Daly[2], and Claudio Paniconi[3]

[1]Department of Civil, Environmental and Architectural Engineering, University of Padua, Padua, Italy, [2]Department of Civil Engineering, Monash University, Melbourne, Victoria, Australia, [3]INRS-ETE, University of Quebec, Quebec City, Quebec, Canada

Abstract In arid and semiarid climate catchments, where annual evapotranspiration (*ET*) and rainfall are typically comparable, modeling *ET* is important for proper assessment of water availability and sustainable land use management. The aim of the present study is to assess different parsimonious schemes for representing *ET* in a process-based model of coupled surface and subsurface flow. A simplified method for computing *ET* based on a switching procedure for the boundary conditions of the Richards equation at the soil surface is compared to a sink term approach that includes root water uptake, root distribution, root water compensation, and water and oxygen stress. The study site for the analysis is a small pasture catchment in southeastern Australia. A comprehensive sensitivity analysis carried out on the parameters of the sink term shows that the maximum root depth is the dominant control on catchment-scale *ET* and streamflow. Comparison with the boundary condition switching method demonstrates that this simpler scheme (only one parameter) can successfully reproduce *ET* when the vegetation root depth is shallow (not exceeding approximately 50 cm). For deeper rooting systems, the switching scheme fails to match the *ET* fluxes and is affected by numerical artifacts, generating physically unrealistic soil moisture dynamics. It is further shown that when transpiration is the dominant contribution to *ET*, the inclusion of oxygen stress and root water compensation in the model can have a considerable effect on the estimation of both *ET* and streamflow; this is mostly due to the water fluxes associated with the riparian zone.

1. Introduction

Integrated surface-subsurface hydrological models (ISSHMs) are useful for simulating the terrestrial water cycle and the spatiotemporal variability of its components in catchments with a detailed resolution of topography [*Sebben et al.*, 2013; *Maxwell et al.*, 2014]. ISSHMs commonly feature a Richards equation-based description of variably saturated subsurface flow coupled with a de Saint Venant equation-based description of routing for overland and channel flow [e.g., *VanderKwaak and Loague*, 2001; *Morita and Yen*, 2002; *Panday and Huyakorn*, 2004; *Ivanov et al.*, 2004; *Rigon et al.*, 2006; *Kollet and Maxwell*, 2006; *Weill et al.*, 2009; *Camporese et al.*, 2010; *Shen and Phanikumar*, 2010; *Brunner and Simmons*, 2012; *An and Yu*, 2014]. ISSHMs can simulate the dynamics of distributed variables, such as water table position and soil moisture content, yet streamflow at the catchment outlet has been the main response variable for calibrating and validating these models. However, the ability of ISSHMs to accurately reproduce other hydrological variables and fluxes is becoming increasingly important in applications that involve, for instance, remote sensing data for land surface processes, intensively monitored field and laboratory experiments, and catchments where streamflow is intermittent [e.g., *Vivoni et al.*, 2010; *Xiang et al.*, 2014; *Niu et al.*, 2014a]. In arid and semiarid climates, where rainfall and evapotranspiration (*ET*) roughly balance each other on an annual basis and streams are typically ephemeral, an adequate representation of *ET* is crucial to provide a correct assessment of water availability, in support of sustainable land use and other resource management objectives.

The dominant component of *ET* is often represented by root water uptake [*Jasechko et al.*, 2013; *Coenders-Gerrits et al.*, 2014; *Wang et al.*, 2014], whose accurate mechanistic modeling would require coupling plant transpiration and photosynthesis along with a three-dimensional evolving soil moisture field capable of accounting for interactions among plants [*Manoli et al.*, 2014]. However, models based on precise

representations of root architecture [e.g., *Doussan et al.*, 2006; *Javaux et al.*, 2008; *Kalbacher et al.*, 2011; *Javaux et al.*, 2013; *Manoli et al.*, 2014] are not yet feasible for large-scale hydrological simulations, due to the difficult parameterization of root architecture for interacting plants and the high computational effort required. Therefore, approaches of varying degree of complexity, typically relying on a vertically distributed root water uptake approximation, are used in existing ISSHMs to describe ET. Perhaps the simplest scheme is based on boundary condition (BC) switching [*Camporese et al.*, 2010], whereby a single threshold parameter marks the transition between atmosphere-controlled evaporation, equal to the potential rate, and soil-limited evaporation in water stress conditions. A popular macroscopic approach that explicitly accounts for vegetation uses a sink term to represent the root system and calculates root water uptake from different soil layers as a function of potential evapotranspiration, ET_p, root density distribution, and soil moisture content [*Skaggs et al.*, 2006; *Šimůnek et al.*, 2013]. Potential evapotranspiration is distributed over the root depth according to the root density to calculate the potential root water uptake; the actual root water uptake is assumed to be a fraction of the potential uptake expressed as a function of the water content at different depths. The sum of the contributions to actual root water uptake over different depths yields the actual evapotranspiration, ET_a. A common formulation to estimate actual root water uptake from its potential value is the Feddes reduction function [*Feddes et al.*, 1976, 1978]. Some ISSHMs use variations of the Feddes function [*Heppner et al.*, 2007; *Shen and Phanikumar*, 2010], while others embed the calculation of ET_a within the surface energy balance [*Ivanov et al.*, 2004; *Rigon et al.*, 2006]. More recently, some ISSHMs have been coupled to land surface models, thereby integrating subsurface flow and surface routing to energy, water, and carbon flux exchanges between the land surface and the atmosphere [*Ivanov et al.*, 2008; *Kollet and Maxwell*, 2008; *Shen et al.*, 2013; *Niu et al.*, 2014b].

Although the approaches based on sink terms, and in particular the Feddes reduction function, can easily account for oxygen stress, i.e., reduction of root water uptake in waterlogged soils due to lack of oxygen [*Bartholomeus et al.*, 2008], and root water compensation, i.e., the ability of plants to adjust their distribution of water uptake along the soil profile as a function of local soil water content [e.g., *Jarvis*, 1989; *Verma et al.*, 2014], their impact on the catchment water balance has never been evaluated in applications of ISSHMs.

In this paper, we compare two methods for modeling ET, studying the effects of these methods on the simulation of catchment-scale hydrological fluxes within the Catchment Hydrology (CATHY) model [*Camporese et al.*, 2010]. As shown in *Camporese et al.* [2014], the BC switching can be effectively used to reproduce ET fluxes in catchments with shallow rooted vegetation. The limitations of this method when modeling catchments with deeper root systems are discussed here. An alternative model, which describes water uptake over the root depth, was thus implemented in CATHY, and the role of the parameters involved is discussed in detail. The two schemes are selected because both are parsimonious and can be implemented into existing flow models without the added effort and parametric complexity of integrating energy and carbon balance equations or root system architecture into the model. The analysis was carried out for a semiarid catchment in southeastern Australia, already investigated in *Camporese et al.* [2014]. In addition to comparing the two schemes, the roles of oxygen stress and root water compensation in driving ET_a and streamflow at the catchment scale are discussed.

2. Methods

2.1. Site Description

The study area (Figure 1) is a 0.48 km^2 catchment located in Mirranatwa, southwest Victoria (Australia). The catchment is predominantly used as pasture for sheep and its subsurface consists of a granite aquifer with well-weathered, porous, permeable saprolite in the upper 10–20 m and a relatively fresh and fractured bedrock below 20 m [*Hergt et al.*, 2007; *VandenBerg*, 2009]. The topography of the site suggests that the catchment is a local system, with negligible regional groundwater input [*Dean et al.*, 2015]. Of 13 bores drilled to varying depth, eight are equipped with data loggers that record groundwater levels at a 4 h time interval, but only three of them (B2274, B2275, B2296 in Figure 1) are screened at depths relevant for this study [*Camporese et al.*, 2014]. A V-notch weir located at the outlet of the catchment (adjacent to bore B2296) measures streamflow at 30 min intervals. An eddy covariance station was in operation from March 2012 to February 2013, providing almost 1 year of actual evapotranspiration measurements. Daily rainfall and atmospheric temperature data are available from nearby weather stations located at Mirranatwa and
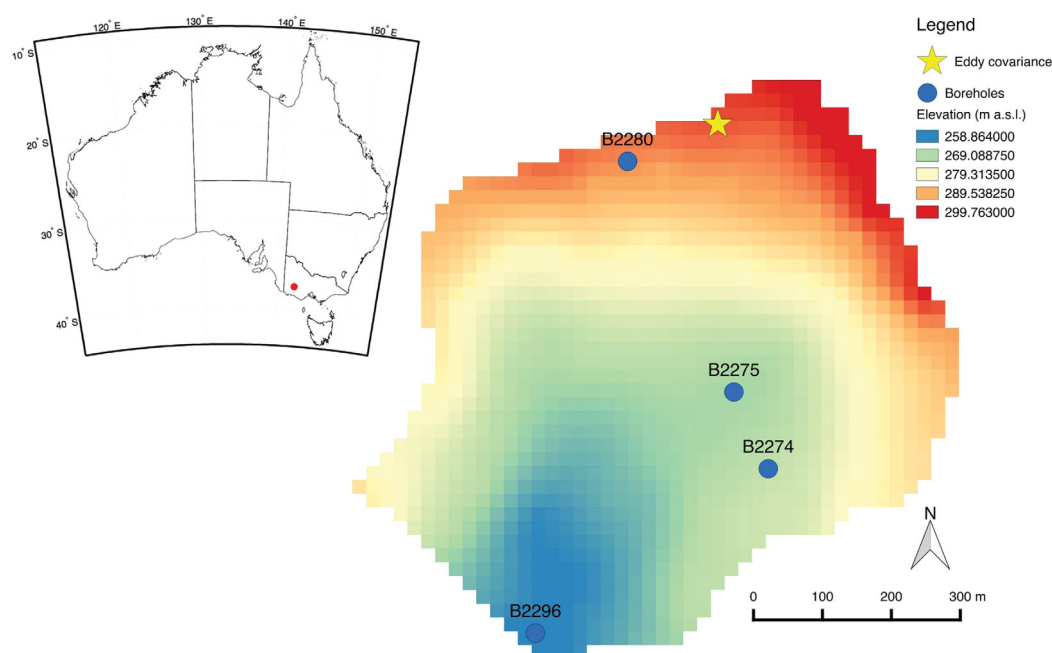
Figure 1. (left) Location of the study catchment within Australia and (right) 20 m resolution digital elevation model with monitoring bore-holes and the location of the eddy covariance station. Observations in bores B2274, B2275, and B2296 are compared to the simulations to assess the model performance, while the location of bore B2280 is used for analyses reported in sections 3.3 and 3.4.

Hamilton, respectively; both stations are operated by the Bureau of Meteorology (station numbers 089019 and 090173, www.bom.gov.au). The average annual rainfall for the period 1901–2013 was 672 mm, while the average annual pan evaporation (Class A) was estimated at about 1350 mm [*Dean et al.*, 2015]. A further description of the site and installed instrumentation can be found in *Camporese et al.* [2014] and *Dean et al.* [2015].

2.2. Model Description and *ET* Schemes

The CATHY model combines the three-dimensional (3-D) Richards equation for subsurface flow in variably saturated porous media with a one-dimensional diffusion wave approximation of the de Saint Venant equations for surface water dynamics [*Camporese et al.*, 2010]. Forced by rainfall and potential evapotranspiration at the soil surface, the model output includes spatially distributed quantities (e.g., moisture content, surface and subsurface flow velocities, aquifer water levels, and ponding heads) and integral quantities (e.g., streamflow at the catchment outlet and total groundwater storage). To take into account surface roughness and microtopography, surface flow occurs when a minimum water depth (h_{min}) on the surface is exceeded. Overland flow is assumed to concentrate in rills or rivulets confined to hillslope cells, while channel flow occurs on stream cells [*Orlandini et al.*, 2003; *Camporese et al.*, 2010]. Input for the model, besides atmospheric forcing, includes surface flow parameters, such as Gauckler-Strickler conductance coefficients for hillslopes and channels, and subsurface properties, such as saturated hydraulic conductivity and soil retention curves. CATHY uses an adaptive time stepping strategy, whereby time steps are adjusted within a user-defined range on the basis of the number of iterations required to achieve convergence of the nonlinear subsurface module [*D'Haese et al.*, 2007]. Further details on the numerical methods used to solve the equations can be found in *Paniconi and Putti* [1994] and *Orlandini and Rosso* [1998].

CATHY can model evapotranspiration in two different ways. The first method is based on the original formulation for modeling soil evaporation [*Camporese et al.*, 2010]. Evaporation from the soil surface is calculated with a procedure that switches the boundary condition between prescribed flux (Neumann condition) and water pressure head (Dirichlet condition) depending on the water pressure head of the nodes at the surface. As long as the water pressure head at the soil surface is larger than a threshold value, Ψ_{min}, the boundary condition is a flux that equals the potential evaporation rate. When the water pressure head at the surface reaches Ψ_{min}, the boundary condition switches from a flux to a constant pressure head, equal to

Ψ_{min}, and the flux becomes soil limited. Although this method was developed to model soil evaporation, it has been shown that with a proper calibration of Ψ_{min}, the evaporative fluxes at the surface can be interpreted as evapotranspiration from catchments with shallow rooted vegetation [*Camporese et al.*, 2014]. We refer to this *ET* scheme as BC switching.

The second method, which is a simplification of the model implemented in CATHY by *Niu et al.* [2014b], includes a sink term (*S*) in the Richards equation to account for root water uptake varying with depth [*Šimůnek et al.*, 2013]. The potential transpiration is distributed across the root depth as a function of the root distribution, $\beta(z)$, expressed as [*Vrugt et al.*, 2001]:

$$\beta(z) = \left[1 - \frac{z}{z_m}\right] e^{-\frac{p_z}{z_m}z},$$ (1)

where *z* is depth (i.e., positive downward), z_m is the maximum rooting depth, and p_z is an empirical parameter. Transpiration depends on the soil water content in the root zone. If the soil is dry, vegetation can experience water stress and transpiration reduces to limit water losses; in nearly saturated conditions, the low availability of oxygen to roots might also cause a decrease in transpiration rates. The effect of low and high soil moisture, θ, on root water uptake, and thus transpiration, is commonly modeled by multiplying the potential root water uptake by a reduction function, α (Figure 2) [*Feddes et al.*, 1976]. The reduction function, commonly referred to as the Feddes function, is zero at saturation, when oxygen stress is inhibiting root water uptake. As θ decreases, α is assumed to increase linearly up to 1 at the anaerobiosis point (θ_{an}). When soil moisture falls below θ_d, associated with incipient water stress, transpiration is assumed to decrease linearly, reaching zero at the wilting point, θ_{wp}. Between θ_{an} and θ_d, the soil is in well-watered conditions and roots can take up water at the potential rate (i.e., $\alpha = 1$). Other reduction functions have been proposed in the literature to account for nonlinearities in the relationship between soil moisture and water stress [*Metselaar and De Jong Van Lier*, 2007] and to improve the estimate of θ_{an} when considering oxygen stress [*Bartholomeus et al.*, 2008]. Because of its wide use, and because it requires fewer parameters, we use in this work a function with linear reductions for both water and oxygen stress and a constant value of θ_{an} [*Feddes et al.*, 1976].

The sink term, which represents actual root water uptake rate at the *i*th node along each vertical series of nodes in the 3-D grid, can thus be calculated as

$$S(z_i) = \alpha(\theta_i) \frac{\beta(z_i)\Delta z_i}{\sum_{i=1}^{m} \beta(z_i)\Delta z_i} ET_p,$$ (2)

where Δz_i is the layer thickness associated with the *i*th node, and *m* is the total number of nodes along the vertical direction with depth not exceeding z_m. When using this method to calculate evapotranspiration, we assumed that evaporation from bare soil was negligible compared to transpiration. In arid and semiarid environments, values for the ratio of transpiration over total evapotranspiration have been reported as high as 80–95% [*Moran et al.*, 2009; *Wang et al.*, 2014]. Although other studies report values as low as 7% [*Reynolds et al.*, 2000], we do not account for soil evaporation in this study because our goal is to clearly distinguish two methods to describe *ET*: the BC switching, which only accounts for water fluxes at the soil surface, and the root water uptake model, which accounts for water fluxes across the soil depth interested by the root system.

Compensatory mechanisms for root water uptake can be taken into account using the model introduced by *Jarvis* [1989] [see also *Šimůnek and Hopmans*, 2009; *Jarvis*, 2010, 2011]. Accordingly, the water stress index, $0 \leq \omega \leq 1$, defined as

$$\omega = \frac{ET_a}{ET_p} = \frac{\sum_{i=1}^{m} \alpha(\theta_i)\beta(z_i)\Delta z_i}{\sum_{i=1}^{m} \beta(z_i)\Delta z_i},$$ (3)

is introduced to characterize the water stress of the whole plant. When ω is larger than a critical value, ω_c, the vegetation is able to redistribute root water uptake over the root depth to maintain transpiration at the potential rate, ET_p. When ω becomes lower than ω_c, the vegetation starts suffering from water stress and the actual transpiration falls below ET_p, decreasing linearly with ω.
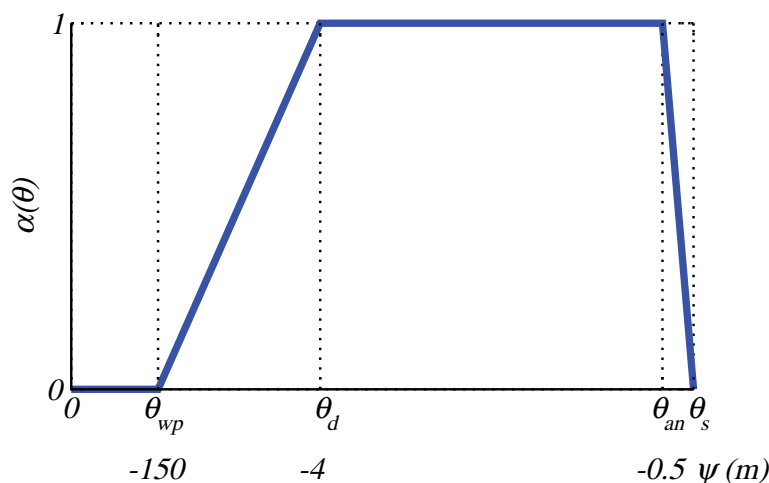
Figure 2. F*eddes et al.* [1976] function for the reduction of root water uptake due to water and oxygen stress. Typical values of pressure head corresponding to the model parameters in terms of soil moisture are reported under the horizontal axis.

When accounting for root water compensation, the sink term can thus be written as

$$S_c(z_i) = \alpha(\theta_i) \frac{\beta(z_i)\Delta z_i}{\sum_{i=1}^{m} \beta(z_i)\Delta z_i} \frac{ET_p}{\max(\omega, \omega_c)}. \tag{4}$$

When $\omega_c = 1$, equations (2) and (4) coincide and there is no compensation; in the extreme (and theoretically undefined) case $\omega_c = 0$, transpiration always occurs at the potential rate, sustained by the part of the root system in the wetter areas of the soil.

2.3. Model Setup and Parameter Calibration

Starting from a 20 m × 20 m resolution digital elevation model (DEM) (Figure 1), a 3-D subsurface grid was constructed by subdividing each DEM cell into two triangles and then projecting this 2-D surface mesh vertically for the total depth of the domain. Based on the geology at the site, the soil depth was assumed to be 10 m, and this depth was discretized into 16 vertical layers. The thickness of the layers varies with depth, starting from 0.05 m at the surface, where a fine mesh is needed to accurately resolve the strong nonlinearities associated with water fluxes near the soil surface, and reaching a maximum thickness of 2.0 m at the bottom of the soil domain. The resulting 3-D grid consists of 22,066 nodes and 116,160 tetrahedral elements.

Calibration of the model was performed using data collected from 16 February 2011 to 15 February 2012, while model validation was performed against data from 16 February 2012 to 31 January 2013. The atmospheric boundary conditions consisted of measured daily rainfall and estimated ET_p, which was calculated from air temperature data using the Hargreaves-Samani formula [*Hargreaves and Samani*, 1982; *Camporese et al.*, 2014]. Daily atmospheric inputs were uniformly distributed across 24 h for each day of the simulations, while the maximum time step was set to 6 h, meaning that short-term processes such as infiltration excess runoff and *ET* daily cycles were not taken into account. We focus here on the annual water budget, for which these short-term dynamics are less relevant. Consistent with the hypothesis of the catchment as a local system and the absence of regional groundwater inputs [*Dean et al.*, 2015], no-flow conditions were assigned to the bottom of the grid and to all lateral boundaries. The initial conditions for the calibration were generated by running a warm-up period for the previous 10 years, using measured rainfall rates and estimated ET_p fluxes. The warm-up period was long enough to obtain an initial state for the calibration run that was independent of the arbitrary conditions assigned at the beginning of the warm-up simulation. The water pressure head profiles and surface discharge at the end of the warm-up period were then used as initial conditions for the calibration simulation, while the states at the end of the calibration provided the initial conditions for the validation simulation.

The model was calibrated and validated against observed streamflow and further assessed by comparing modeled and measured groundwater levels and actual *ET*. Model parameters were assigned as described in *Camporese et al.* [2014] and are reported in Table 1. The only parameters that needed calibration to achieve

Table 1. Values of the Main Parameters Used in the Calibration and Validation Simulations

Model Parameter	Value
Saturated hydraulic conductivity (K)[a]	$K = 1.01 \times 10^{-5} z^{-0.27}$ m s^{-1}
Specific storage coefficient (S_s)	1.0×10^{-3} m^{-1}
Porosity (θ_s)	0.40
van Genuchten [1980] coefficients (θ_r, α, n)	0.03, 1.85 m^{-1}, 1.52
Gauckler-Strickler Conductance Coefficient (GS)	
Channel	10 m$^{1/3}$ s^{-1}
Hillslope	1 m$^{1/3}$ s^{-1}
Minimum ponding head (h_{min})[b]	4.0×10^{-4} m
Root water uptake parameters	0.40, 0.16, 0.06, 0, 0.4 m
(θ_{an}, θ_d, θ_{wp}, p_z, z_m)[b]	
Critical water stress index (ω_c)	1

[a]z denotes depth from the ground surface (positive downward).
[b]Calibrated.

a satisfactory match between simulated and observed streamflow were h_{min} and the parameters of the Feddes function. Parameter calibration was only carried out for the model with the root sink term.

A sensitivity analysis was carried out by *Camporese et al.* [2014] to investigate the dependence of ET_a and streamflow on the parameter Ψ_{min} of the BC switching scheme. To compare the two approaches for computing ET_a, a similar sensitivity analysis was performed for the parameters of the sink term scheme. For this analysis, we used the same initial and boundary conditions and model parameters as the validation simulation. Only the parameters of the Feddes function were varied, one at a time, according to the values reported in Table 2, for a total of 24 simulations on top of the validation run.

The catchment used in the study is in a dry climate, where precipitation is almost completely balanced by ET. To extend our results and conclusions to different climatic conditions, we ran additional simulations for a hypothetical wetter scenario, where rainfall was increased by 50% for both the warm-up period and the analysis simulations. We will refer to these two different cases as the dry and wet scenarios.

3. Results

3.1. Model Calibration and Validation

A minimum water ponding (h_{min}) of 4×10^{-4} m provided a good fit between simulated and observed streamflow (Figure 3b), with values of the Willmott index of agreement [*Willmott*, 1981] ranging from 0.90 in calibration to 0.88 in validation, coefficients of determination (R^2) larger than 0.63, and root mean square errors not exceeding 0.09 mm d^{-1} (Table 3). The calibrated value of h_{min} is slightly different from that reported in *Camporese et al.* [2014], because in the present study, we used depth-variable root water uptake for both calibration and validation instead of BC switching driven by Ψ_{min}. The values of the parameters in the root water uptake model were within the ranges suggested by *Feddes et al.* [1976]. Table 3 also reports indices of model performance for water table levels in a few representative boreholes and ET_a. Considering that the model was calibrated exclusively against streamflow data, the ability of the model to reproduce measured annual ET_a was deemed satisfactory for the purpose of this study (Figure 3c and Table 3). Some model underestimation in winter and overestimation in summer may be due to the fact that the root water uptake parameters were kept constant throughout the simulations, while typically the grass grows in winter and partially wilts in summer. The ET_a data could perhaps be better reproduced using more complex ET_p formulations (e.g., Penman-Monteith) than the Hargreaves-Samani formula, which was selected based on availability of air temperature data. Figure 3 also reports the results of an uncalibrated simulation carried out using the BC switching scheme with a value of Ψ_{min} equal to -128 m. Overall, Table 3 and Figure 3 demonstrate that the model captures well the annual hydrological dynamics of the catchment.

3.2. Sensitivity Analysis

Figure 4 shows the results of the sensitivity analysis in terms of cumulative ET_a and streamflow percent change as

Table 2. Values of the Parameters Used for the Sink Term Model Sensitivity Analysis and Comparison With BC Switching

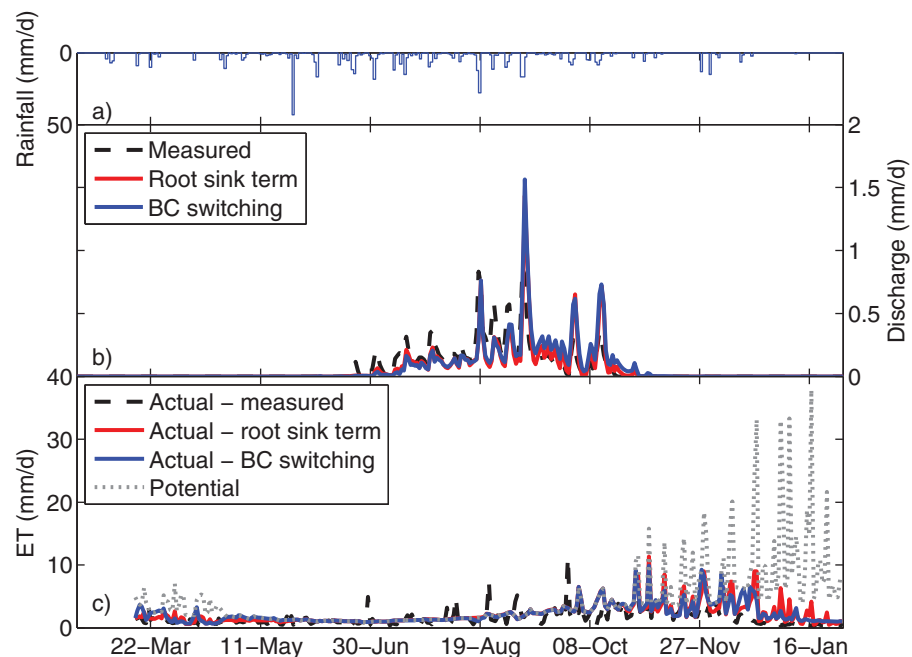| Parameter	Values				
	Run 1	Run 2	Run 3	Run 4	Run 5
Root Sink Term					
θ_d	0.08	0.12	0.16	0.20	0.24
z_m (m)	0.2	0.4	0.8	1.6	3.2
p_z	0	1	2	5	10
θ_{an}	0.32	0.34	0.36	0.38	0.40
θ_{wp}	0.06	0.08	0.10	0.12	0.14
ω_c	0.025	0.25	0.50	0.75	1.00
BC Switching					
Ψ_{min} (m)	-32	-64	-128	-256	-512

Figure 3. Comparison between observed and simulated (b) streamflow and (c) evapotranspiration for the validation period (from 16 February 2012 to 31 January 2013), with input rainfall rate reported in Figure 3a. Observed *ET* data are only available from 15 March 2012. The uncalibrated simulation with the BC switching method was carried out using $\Psi_{min} = -128$ m.

a function of standardized parameter percent change. The standardized percent change of a parameter (e.g., θ_d) was calculated as the difference between the value of the parameter in a particular run (Table 2) and the central value of the same parameter (e.g., $\theta_d = 0.16$ for Run 3 in Table 2); this difference was then divided by the total range of variation of the parameter (e.g., Table 2; $\Delta\theta_d = 0.24 - 0.08$) [*Pannell*, 1997]. The analysis points out that the primary control for both ET_a and streamflow is the maximum root depth z_m, followed by θ_d and θ_{wp}. The shape of the root depth distribution, controlled by p_z, had a minor effect, while θ_{an} was significant only when it switched oxygen stress on, i.e., when it varied from 0.40 (no oxygen stress) to 0.38. Further decreases of θ_{an} had minor impacts on the catchment water balance. Similarly, the critical water stress index ω_c had a more significant impact than θ_d and θ_{wp} only when approaching 0 (i.e., $\omega_c = 0.025$). All the parameters had a relatively larger impact on streamflow compared to *ET*, due to the small magnitude of the former term (around 4% of ET_a) and thus larger percent change for the same absolute variations.

The sensitivity analysis, limited to the parameters z_m, θ_{an}, and ω_c, was repeated for the wet scenario. All other inputs were the same as in the validation simulation. The results are reported in Figure 5, where they are compared with those for the dry scenario. The maximum root depth, z_m, is still the primary control, especially on ET_a, although the sensitivity for the wet scenario is smaller due to the less frequent occurrence of water stress conditions. The sensitivity to θ_{an} also shows a pattern similar to the dry scenario, but with different magnitude. As in the previous case, differences in ET_a and streamflow are evident between the case without and

Table 3. Indices of Goodness-of-Fit Between Modeled and Measured Streamflow, Water Table Levels, and Actual *ET* for the Calibration and Validation Runs[a]

	Calibration			Validation		
	WIA	R^2	RMSE	WIA	R^2	RMSE
Streamflow (mm d^{-1})	0.90	0.66	0.06	0.88	0.63	0.09
B2274 (m)	0.22	0.84	1.47	0.20	0.84	1.70
B2275 (m)	0.28	0.18	0.76	0.29	0.27	1.10
B2296 (m)	0.86	0.81	0.39	0.89	0.81	0.54
Actual *ET* (mm d^{-1})[b]	N/A	N/A	N/A	0.62	0.20	1.68

[a]WIA = *Willmott* [1981] index of agreement, R^2 = coefficient of determination, RMSE = root-mean-square error; the results shown are for the sink term model; results for calibration and validation obtained with the BC switching procedure are reported in *Camporese et al.* [2014].

[b]N/A = not available (actual *ET* measurements are only available for the validation period).
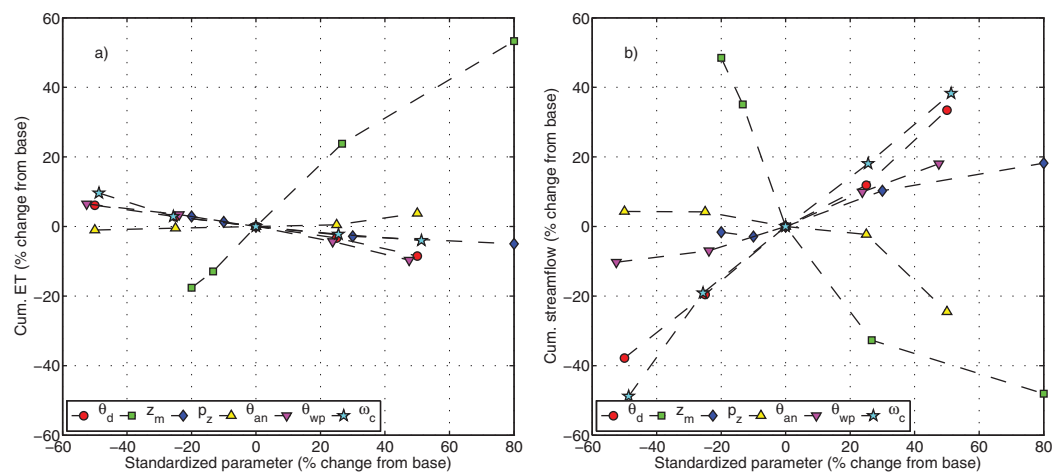
Figure 4. Sensitivity of (a) cumulative evapotranspiration, ET_a, and (b) streamflow to the parameters of the sink term model in the dry scenario.

with oxygen stress, but lowering θ_{an} does not generate any appreciable additional reduction of ET_a or increase in streamflow. The effect of the presence of oxygen stress is more pronounced as a larger portion of the catchment becomes wetter. The sensitivity of cumulative ET_a on ω_c does not change from the dry to the wet scenario, while, similar to z_m, the sensitivity of streamflow decreases, due to higher soil moisture content and less frequent periods of water stress.

3.3. Comparison of BC Switching and Sink Term Schemes

For a direct comparison between fluxes computed through the BC switching and sink term schemes, we show in Figure 6 the cumulative ET and streamflow as a function of Ψ_{min} and z_m for both the dry and wet scenarios. The values of Ψ_{min} used for the comparison are also shown in Table 2. The fluxes are shown as interval ranges corresponding to an uncertainty of $\pm 5\%$ with respect to the values computed by the model.

Figure 6a shows that overlapping of cumulative ET_a occurs for values of maximum root depth smaller than approximately 0.5 m, with corresponding values of Ψ_{min} larger (i.e., closer to zero) than -100 m. More negative values of minimum pressure head are not only unrealistic when compared to the chart proposed by Feddes (Figure 2), but also cannot keep up with the increased root water uptake caused by larger values of root depth. Even though no overlap is detected in Figure 6b for cumulative streamflow, the catchment response is not very different between the two models for the same range of Ψ_{min} and z_m values found for overlapping ET_a, as shown previously in Figure 3. Changes in Ψ_{min} and z_m have similar effects on groundwater recharge. Subsurface storage changes are well correlated with ET_a, which is the dominant catchment water loss. As a result, recharge is more sensitive to z_m in the root sink term approach than Ψ_{min} in the BC switching scheme, and overlap occurs again (not shown) only for z_m smaller than 0.5 m and Ψ_{min} not smaller than -100 m.

Analogous to Figures 6a and 6b, Figures 6c and 6d show that, although both fluxes are now larger in magnitude, due to higher water availability in the wet scenario, ET calculated with the two methods is similar when z_m does not exceed 0.5 m and Ψ_{min} is not smaller than approximately -100 m.

For a closer investigation of the processes occurring in the root zone, Figure 7 shows the modeled soil moisture evolution at two depths (28 and 90 cm) in the location of borehole 2280, and for values of Ψ_{min} and z_m in the range where ET_a calculated with the two methods overlaps (i.e., $\Psi_{min} = -64$ m and $z_m = 0.4$ m) and where it does not overlap ($\Psi_{min} = -512$ m and $z_m = 3.2$ m). Figures 7a and 7c demonstrate that, as long as the root depth is smaller than 0.5 m, soil moisture in the root zone profile calculated with the two methods is similar. This suggests that, for shallow rooted vegetation, a single-parameter, surface boundary-controlled calculation of evapotranspiration performs as well as the root water uptake model in terms of both ET_a (Figure 6a) and soil moisture dynamics.

This result did not extend to the case of vegetation with deep root systems. Figures 7b and 7d show that decreasing Ψ_{min} to match the ET_a obtained for deeper root distributions led to very different soil
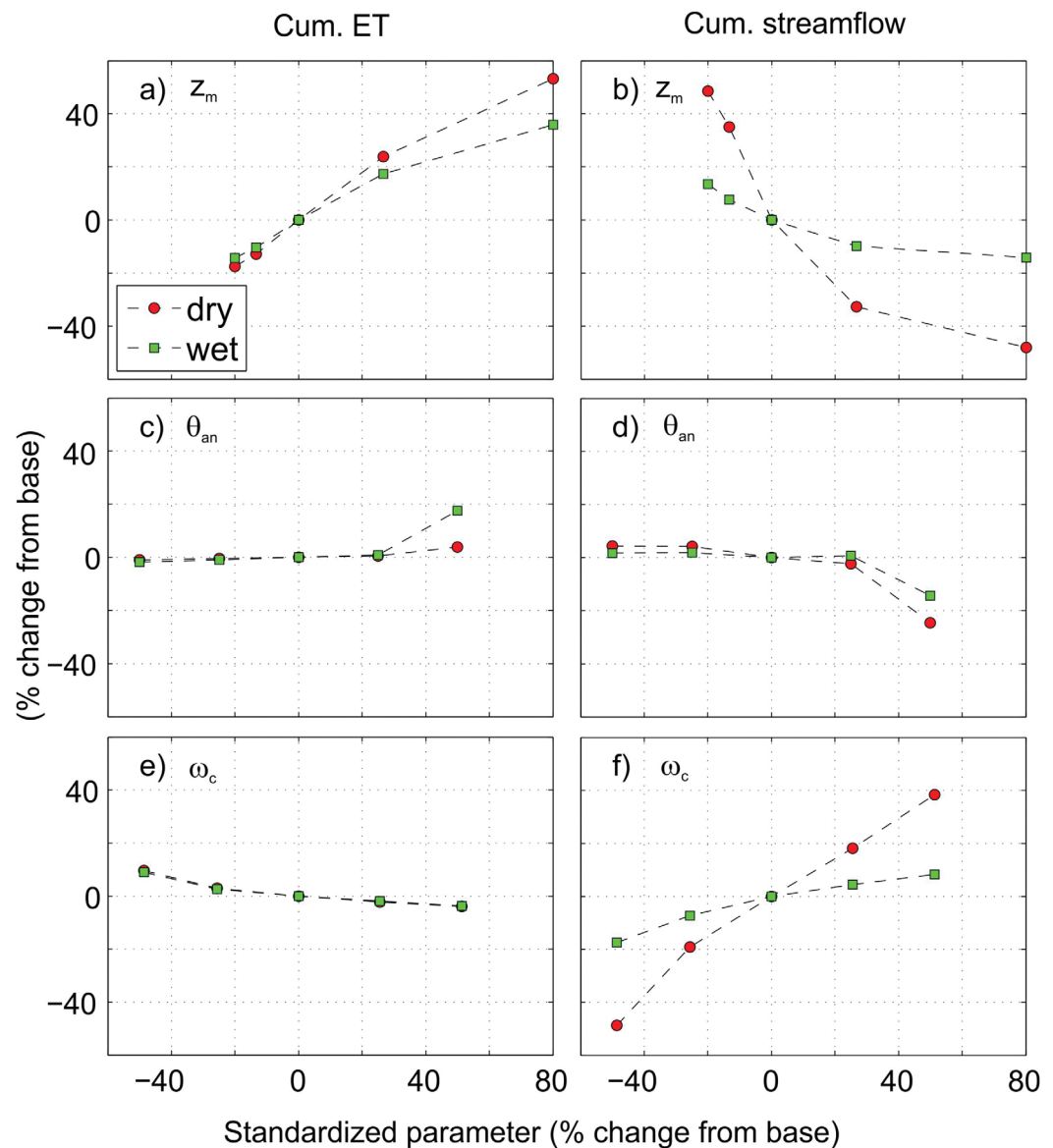
Figure 5. Sensitivity of (a, c, and e) cumulative ET_a and (b, d, and f) streamflow on (a and b) z_m, (c and d) θ_{an}, and (e and f) ω_c for the dry and wet scenarios.

moisture profiles. Very low and unrealistic values of Ψ_{min} tended to dry the soil surface very quickly, thereby reducing percolation and groundwater recharge. Accordingly, the seasonal cycle of soil moisture could not be reproduced and soil moisture at different depths remained fairly constant throughout the year. When compared to the results obtained with the sink term reduction function, soil moisture calculated with BC switching tended to be larger in summer, because of the lower ET_a rates, and much lower in winter, because of the fast evaporation from the surface after rainfall events. Low values of Ψ_{min} also caused numerical artifacts, as shown by sudden soil moisture drops after rainfall events toward the beginning of autumn (about day 100 in Figure 7d) and spring (about day 270 in Figure 7b). This is due to sharp switches from ET to rainfall and then again to ET; in such cases, the soil surface is initially extremely dry (pressure head around or equal to Ψ_{min}) and the wetting front produced by the rain cannot propagate to deeper soil layers because of very low values of hydraulic conductivity. After the rain, the soil surface is still unsaturated but with pressure head larger than Ψ_{min}, resulting in high evaporation fluxes (equal to the potential rates) that eventually propagate downward and cause delayed decreases in soil moisture.
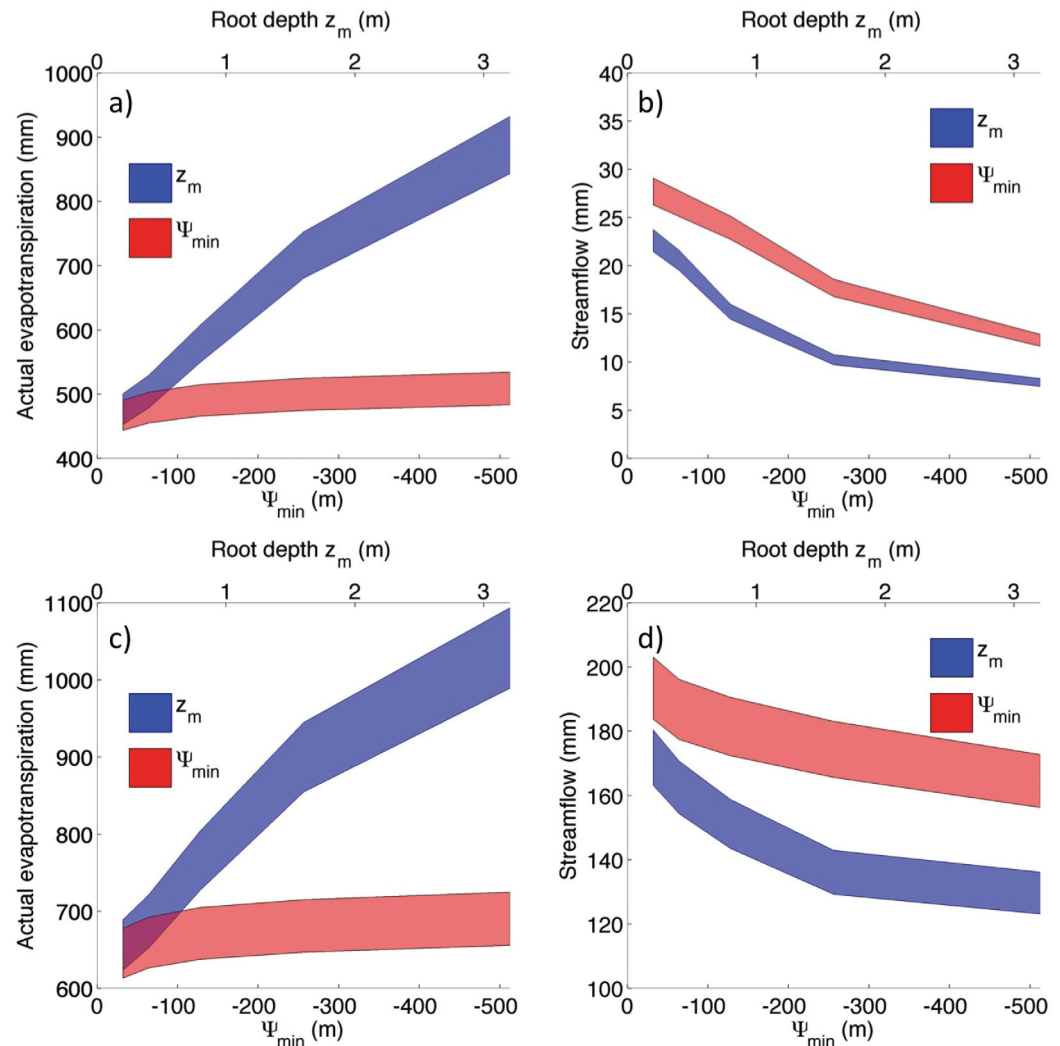
Figure 6. (a and c) Cumulative ET_a and (b and d) streamflow) as a function of Ψ_{min} and maximum root depth (z_m) in the (a and b) dry and (c and d) wet scenarios. Filled regions represent uncertainty intervals computed as ±5% of the model output.

Figure 8 shows the full vertical profiles of soil moisture at the same location (borehole 2280) and for the same values of Ψ_{min} and z_m immediately after a major rainfall event and after a prolonged dry period. The comparison between the profiles for $\Psi_{min} = -64$ m and $z_m = 0.4$ m confirms that the soil moisture dynamics modeled with the two methods are similar for shallow rooted vegetation (about 0.5 m), while they are strongly mismatched for vegetation with depeer root systems.

The comparison between the BC switching and sink term schemes is completed by a look at the computational time required by the model to complete the simulations of the sensitivity analysis. Due to the adaptive time stepping strategy, the computational time in CATHY is roughly proportional to the total number of subsurface time steps required to complete the simulation, so we used this number as a proxy for the overall computational effort. Figure 9 shows the total number of subsurface time steps as a function of Ψ_{min} and the sink term scheme parameters for each of the model configurations reported in Table 2. These results refer to the case with measured rainfall (dry scenario); the wet scenario gave similar results.

Consistently with *Camporese et al.* [2014], decreasing Ψ_{min} increased the computational time due to slow convergence of the Richards equation solver for very dry soils. The parameters of the sink term scheme exhibited a similar impact: for instance, as θ_d, θ_{wp}, and ω_c increased, ET_a decreased and so did the number of time steps. A noticeable increase in time steps was caused by increasing p_z, i.e., by progressively concentrating the transpiration flux toward the surface nodes; this effect is not dissimilar to that of Ψ_{min}, even
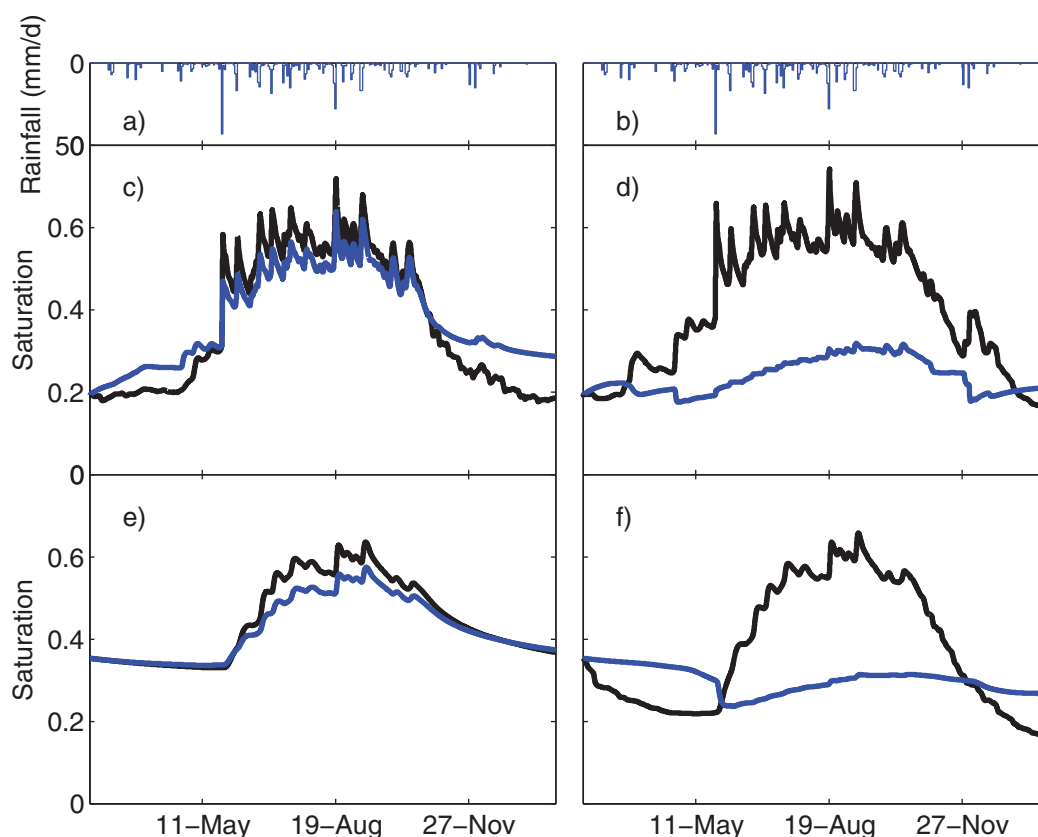
Figure 7. Saturation simulated in the location of borehole 2280 (Figure 1): (c) at 28 cm depth with $z_m = 0.4$ m and $\Psi_{min} = -64$ m; (d) at 28 cm depth with $z_m = 3.2$ m and $\Psi_{min} = -512$ m; (e) at 90 cm depth with $z_m = 0.4$ m and $\Psi_{min} = -64$ m; (f) at 90 cm depth with $z_m = 3.2$ m and $\Psi_{min} = -512$ m. Blue and black lines indicate simulations with the BC switching and sink term schemes, respectively. Figures 7a and 7b report the input rainfall rate.

though not as pronounced. Although increasing the maximum root depth z_m increases ET_a, the computational time decreased, probably due to more evenly distributed outgoing fluxes along the nodes located within the root zone. The activation of oxygen stress (i.e., changing θ_{an} from 0.40 to 0.38) and decreasing the parameter θ_{an} increased dramatically the computational time, probably due to convergence difficulties arising from the coexistence of nodes in the riparian zone that are nearly saturated with an outgoing
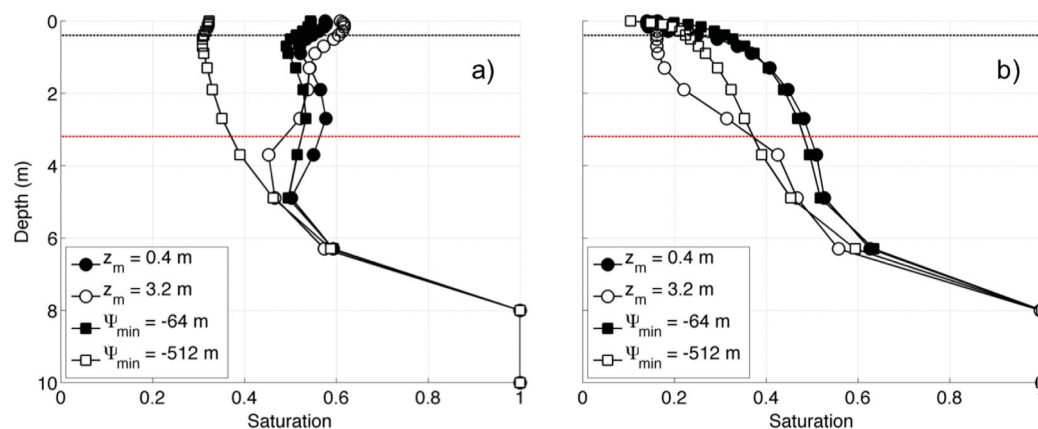

Figure 8. Soil moisture vertical profiles simulated in the location of borehole 2280 (Figure 1) at (a) 240 days (13 October), immediately after a significant rainfall event, and (b) 350 days (31 January), after a prolonged dry period. The two horizontal lines represent the two maximum root depths at 0.4 and 3.2 m.
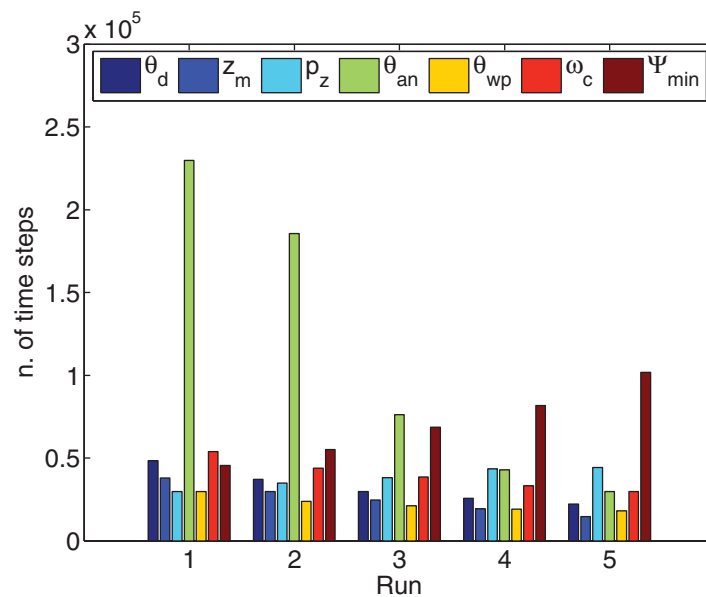
Figure 9. Number of subsurface time steps required to complete model runs in the sensitivity analysis for the dry scenario. Run numbers correspond to the parameter values reported in Table 2.

evaporative flux and that are saturated with a ponding boundary condition. Overall, the computational effort required by the BC switching method is similar to that of the sink term scheme for Ψ_{min} values in a physically meaningful range.

3.4. Roles of Oxygen Stress and Root Water Compensation

The reduction of transpiration associated with oxygen stress and the mechanism of root water compensation can be taken into account by the sink term approach but cannot be reproduced by the BC switching scheme. As reported in section 3.2, activation of oxygen stress (i.e., $\theta_{an} < \theta_s$) not only has a significant impact on ET_a in the wet
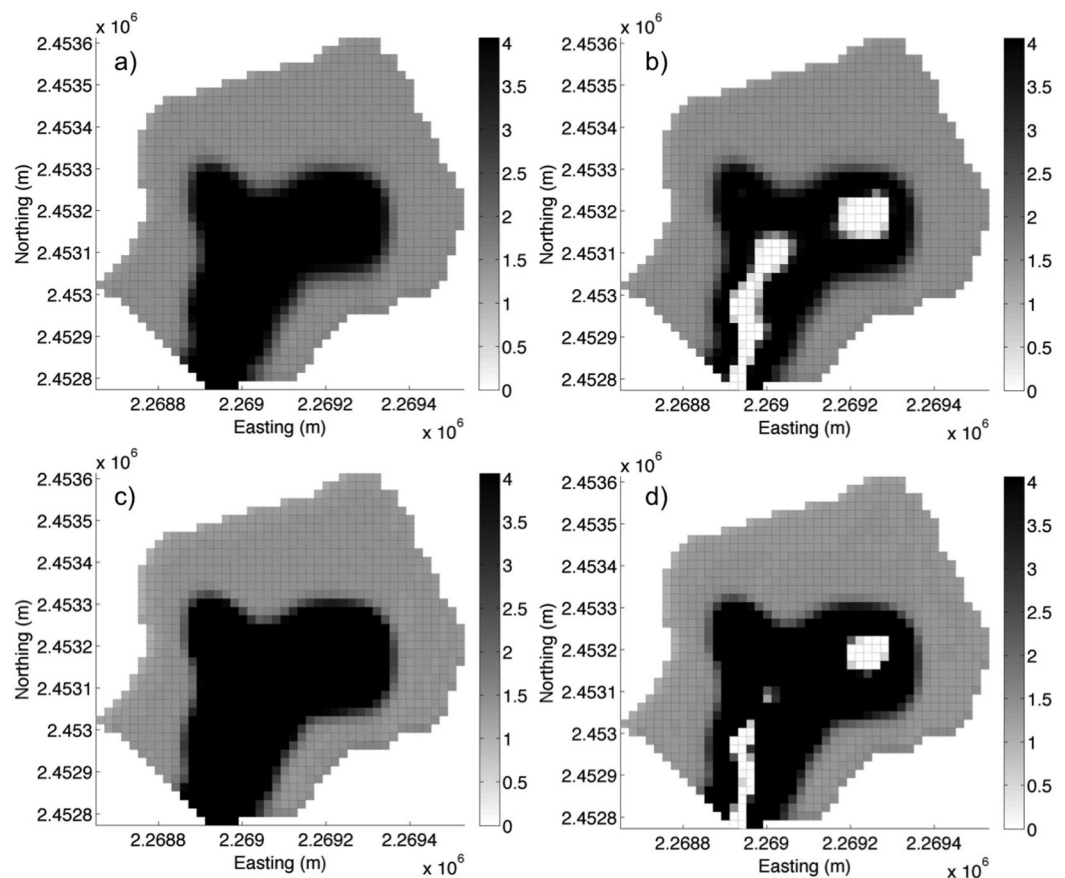

Figure 10. Spatial distribution of ET_a (mm/d) on simulation day 270 (12 November) of the dry scenario with (a) no oxygen stress ($\theta_{an} = \theta_s = 0.40$) and no root water compensation ($\omega_c = 1.0$), (b) oxygen stress ($\theta_{an} = 0.34$) and no root water compensation ($\omega_c = 1.0$), (c) no oxygen stress ($\theta_{an} = \theta_s = 0.40$) and root water compensation ($\omega_c = 0.5$), and (d) oxygen stress ($\theta_{an} = 0.34$) and root water compensation ($\omega_c = 0.5$).
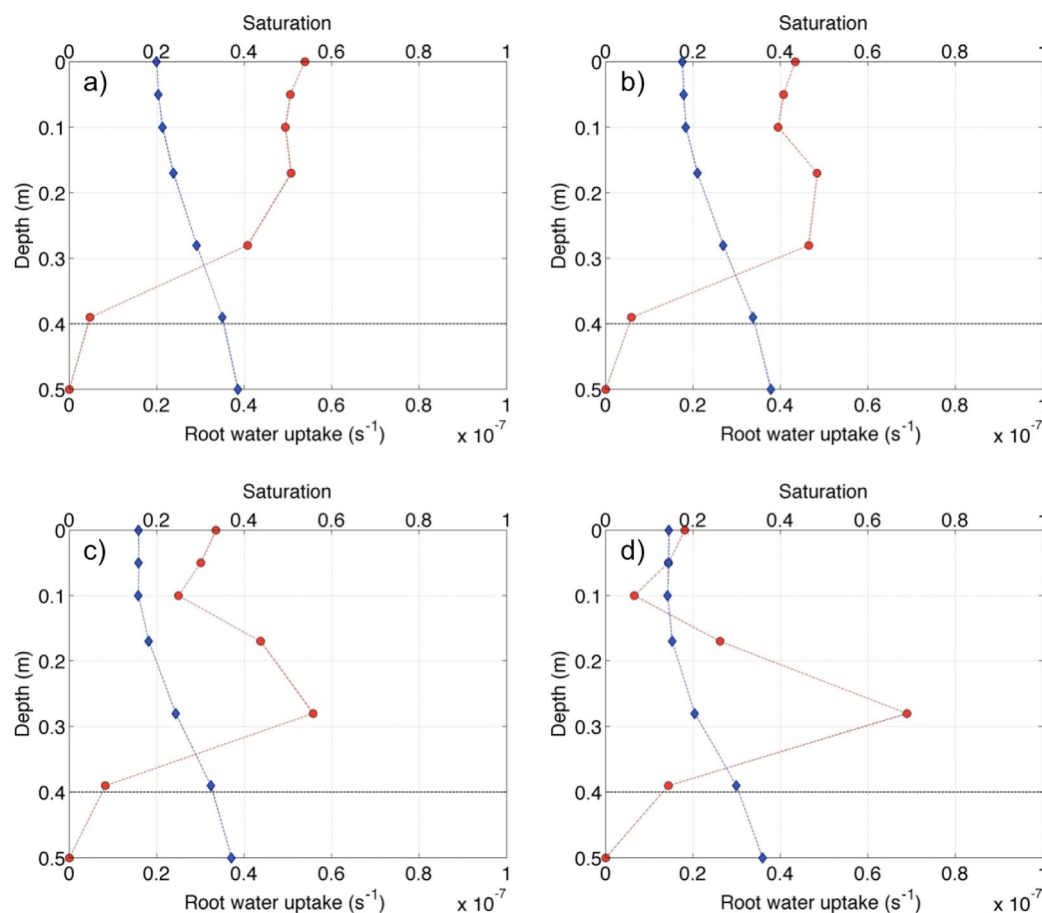
Figure 11. Vertical profiles of saturation and root water uptake in the location of borehole 2280 on simulation day 270 (12 November) of the dry scenario with (a) no root water compensation ($\omega_c = 1.0$), (b) $\omega_c = 0.75$, (c) $\omega_c = 0.5$, and (d) $\omega_c = 0.25$. Red dots and blue diamonds indicate root water uptake and saturation, respectively, while the dashed black line denotes maximum root depth z_m.

scenario, but also on total streamflow for both the dry and wet scenarios (Figures 4 and 5), while root water compensation plays an important role on streamflow, especially in the dry scenario. In addition, the computational time can increase dramatically when oxygen stress is taken into account in CATHY (Figure 9).

Further insights into these processes can be gained by plotting maps of ET_a for different combinations of θ_{an} and ω_c values. The plots in Figure 10 show that the main contribution to actual ET_a comes from the riparian zone, which is more prone to saturation than the hillslopes and thus provides more water to meet the evaporative demand. However, this is also the area within the catchment that is more subjected to oxygen stress, when activated, as shown by the increase in the areas where $ET_a = 0$ (i.e., white parts of the catchment in the figure) as θ_{an} decreased from 0.40 (Figure 10a) to 0.34 (Figure 10b). The fraction of regions affected by oxygen stress is relatively low compared to the total catchment area but significant compared to the saturated area, which is responsible for the generation of streamflow. For this reason, the percentage impact of decreasing θ_{an} on cumulative ET in the dry scenario (504 versus 483 mm, for $\theta_{an} = 0.40$ and 0.34, respectively) is not as strong as the impact on streamflow (21 versus 28 mm). On the other hand, in the wet scenario, the effects of changing θ_{an} on cumulative ET (687 versus 578 mm) and streamflow (163 versus 193 mm) are similar, because in this case the fraction of saturated area is much larger than in the case with measured rainfall data.

A close comparison between Figure 10a and Figure 10c, i.e., $\omega_c = 1.0$ versus $\omega_c = 0.5$, highlights a small but visible increase in the size of the black region, i.e., where actual ET rates are maximal. This is clearly due to the activation of root water compensation, which plays an important role at the outer limits of the riparian zone, where surface soil moisture gradually declines but deeper soil layers can still sustain high evapotranspiration rates.

A combination of the impacts due to oxygen stress and root water compensation is shown in Figure 10d, which exhibits a significant reduction of white regions thanks to the compensatory effect of increased root water uptake from alternative soil layers.

Note that these analyses are only valid under the assumption that transpiration is the dominant factor contributing to ET. In fact, even in the case of soil saturation, when transpiration reduces to zero, ET should equal bare soil evaporation if the latter is significant. However, this situation should not be very frequent in our study region, where saturation mainly occurs in winter, when radiation availability at the ground is not high.

To further clarify the role of root water compensation on catchment dynamics, we show in Figure 11 the simulated vertical profiles of saturation and root water uptake at borehole 2280 on simulation day 270 (12 November) of the dry scenario. The figure shows how the root uptake moves deeper into the profile, where the soil is wetter, as ω_c gets smaller. The nonmonotonic behavior of root water uptake with depth is the result of the complex feedback between the root distribution $\beta(z)$ (linear in this case) and soil moisture dynamics.

4. Summary and Conclusions

In a recent study, *Camporese et al.* [2014] showed that a boundary condition switching procedure, implemented in a process-based distributed model, was able to correctly reproduce evapotranspiration (ET) at the catchment scale with only one parameter (a minimum pressure head Ψ_{min}) and by lumping the evapotranspiration fluxes to the surface nodes. In order to investigate under what conditions the assumptions of this method are valid, we compared this simplified approach with the root water uptake model proposed by *Feddes et al.* [1976]. The root water uptake scheme represents the ET process as a sink term in the subsurface hydrological model, and can also account for the reduction of plant transpiration due to oxygen stress and compensatory mechanisms of root water uptake.

The BC switching and sink term schemes are implemented in the CATHY model [*Camporese et al.*, 2010] and tested on a catchment in southeastern Australia. A sensitivity analysis of the sink term reduction function parameters showed that the maximum root depth provides a key control on ET and streamflow, with the soil moisture threshold at incipient water stress and the wilting point also being important. The shape of the root distribution with depth has only a minor effect, while the critical water stress index, which controls root water compensation, exerts a significant influence especially on streamflow. Oxygen stress has an on/off impact, being significant when activated, but with a scarce sensitivity to its soil moisture threshold.

The direct comparison of ET and streamflow computed through the two schemes highlighted that the BC switching procedure is suitable to correctly assess evapotranspiration only for rooting systems shallower than 0.5 m, using values of Ψ_{min} compatible with the range of pressure head values suggested by *Feddes et al.* [1976]. Within this range of applicability, the BC switching method is no more computationally expensive than the sink term scheme and requires the calibration of only one parameter. For deeper rooting systems, the BC switching procedure is unable to match the larger values of ET and is affected by numerical artifacts that prevent a correct reproduction of the drying and wetting processes occurring in the unsaturated zone.

Our analyses were also aimed at investigating the significance of features included in the sink term model that cannot be taken into account by the BC switching procedure, i.e., oxygen stress and root water compensation. We found that these processes can alter significantly the hydrological dynamics in the riparian zone, which is typically the region where streamflow is generated. Therefore, neglecting oxygen stress and/or root water compensation factors may cause significant errors in the modeled water balance of arid and semiarid catchments.

Although the specific results of this study are catchment dependent, some general conclusions, valid for arid and semiarid environments where plant transpiration is the dominant contribution to ET, can be drawn from our analyses. First, the BC switching approach cannot reproduce ET rates from vegetation with deep root systems. Values of Ψ_{min} lower than about -100 m might result in a correct quantification of ET fluxes, but a poor representation of other components of the water balance, such as soil moisture dynamics. In describing the root distribution, root depth is one of the parameters most affecting catchment-scale ET. The parameterization that allows inclusion of oxygen stress affects ET and streamflow, although the soil moisture level defining the onset of oxygen stress is not very important. This is because oxygen stress occurs

mostly along the riparian zone, which is often not very large compared to the size of the catchment. Finally, root water compensation sustains larger *ET* rates and affects the soil moisture profiles, thereby affecting groundwater recharge rates.

Future developments of this research include the application of the two schemes in larger catchments with several vegetation types, which would require the use of a different set of parameters for each vegetation class. While for root water uptake with the Feddes function parameter values are available for a large number of crops [Šimůnek et al., 2013], for the BC switching approach no analogous database of Ψ_{min} values is available and thus this parameter would need to be calibrated for each vegetation class.

References

An, H., and S. Yu (2014), Finite volume integrated surface-subsurface flow modeling on nonorthogonal grids, *Water Resour. Res.*, *50*, 2312–2328, doi:10.1002/2013WR013828.

Bartholomeus, R., J.-P. Witte, P. van Bodegom, J. van Dam, and R. Aerts (2008), Critical soil conditions for oxygen stress to plant roots: Substituting the Feddes-function by a process-based model, *J. Hydrol.*, *360*(1-7), 147–165.

Brunner, P., and C. T. Simmons (2012), HydroGeoSphere: A fully integrated, physically based hydrological model, *Ground Water*, *50*(2), 170–176, doi:10.1111/j.1745-6584.2011.00882.x.

Camporese, M., C. Paniconi, M. Putti, and S. Orlandini (2010), Surface-subsurface flow modeling with path-based runoff routing, boundary condition-based coupling, and assimilation of multisource observation data, *Water Resour. Res.*, *46*, W02512, doi:10.1029/2008WR007536.

Camporese, M., E. Daly, P. E. Dresel, and J. A. Webb (2014), Simplified modeling of catchment-scale evapotranspiration via boundary condition switching, *Adv. Water Resour.*, *69*, 95–105, doi:10.1016/j.advwatres.2014.04.008.

Coenders-Gerrits, A. M. J., R. J. van der Ent, T. A. Bogaard, L. Wang-Erlandsson, M. Hrachowitz, and H. H. G. Savenije (2014), Uncertainties in transpiration estimates, *Nature*, *506*(7487), E1–E2, doi:10.1038/nature12925.

Dean, J. F., J. A. Webb, G. E. Jacobsen, R. Chisari, and P. E. Dresel (2015), A groundwater recharge perspective on locating tree plantations within low-rainfall catchments to limit water resource losses, *Hydrol. Earth Syst. Sci.*, *19*, 1107–1123, doi:10.5194/hess-19–1107-2015.

D'Haese, C. M. F., M. Putti, C. Paniconi, and N. E. C. Verhoest (2007), Assessment of adaptive and heuristic time stepping for variably saturated flow, *Int. J. Numer. Methods Fluids*, *53*(7), 1173–1193, doi:10.1002/fld.1369.

Doussan, C., A. Pierret, E. Garrigues, and L. Pages (2006), Water uptake by plant roots: II—Modelling of water transfer in the soil root-system with explicit account of flow within the root system—Comparison with experiments, *Plant Soil*, *283*(1-2), 99–117, doi:10.1007/s11104-004-7904-z.

Feddes, R. A., P. Kowalik, K. Kolinska-Malinka, and H. Zaradny (1976), Simulation of field water uptake by plants using a soil water dependent root extraction function, *J. Hydrol.*, *31*, 13–26.

Feddes, R. A., P. J. Kowalik, and H. Zaradny (1978), *Simulation of Field Water Use and Crop Yield*, John Wiley, N. Y.

Hargreaves, G. H., and Z. A. Samani (1982), Estimating potential evapo-transpiration, *J. Irrig. Drain. Div. Am. Soc. Civ. Eng.*, *108*(3), 225–230.

Heppner, C. S., K. Loague, and J. E. VanderKwaak (2007), Long-term InHM simulations of hydrologic response and sediment transport for the R-5 catchment, *Earth Surf. Processes Landforms*, *32*, 1273–1292, doi:10.1002/esp.1474.

Hergt, J., J. Woodhead, and A. Schofield (2007), A-type magmatism in the western Lachlan fold belt? A study of granites and rhyolites from the Grampians region, western Victoria, *Lithos*, *97*, 122–139, doi:10.1016/j.lithos.2006.12.008.

Ivanov, V. Y., E. R. Vivoni, R. L. Bras, and D. Entekhabi (2004), Catchment hydrologic response with a fully-distributed triangulated irregular network model, *Water Resour. Res.*, *40*, W11102, doi:10.1029/2004WR003218.

Ivanov, V. Y., R. L. Bras, and E. R. Vivoni (2008), Vegetation-hydrology dynamics in complex terrain of semiarid areas: 1. A mechanistic approach to modeling dynamic feedbacks, *Water Resour. Res.*, *44*, W03429, doi:10.1029/2006WR005588.

Jarvis, N. J. (1989), A simple empirical model of root water-uptake, *J. Hydrol.*, *107*(1-4), 57–72, doi:10.1016/0022-1694(89)90050-4.

Jarvis, N. J. (2010), Comment on "Macroscopic root water uptake distribution using a matric flux potential approach", *Vadose Zone J.*, *9*(2), 499–502, doi:10.2136/vzj2009.0148.

Jarvis, N. J. (2011), Simple physics-based models of compensatory plant water uptake: Concepts and eco-hydrological consequences, *Hydrol. Earth Syst. Sci.*, *15*(11), 3431–3446, doi:10.5194/hess-15-3431-2011.

Jasechko, S., Z. D. Sharp, J. J. Gibson, S. J. Birks, Y. Yi, and P. J. Fawcett (2013), Terrestrial water fluxes dominated by transpiration, *Nature*, *496*(7445), 347–350, doi:10.1038/nature11983.

Javaux, M., T. Schroeder, J. Vanderborght, and H. Vereecken (2008), Use of a three-dimensional detailed modeling approach for predicting root water uptake, *Vadose Zone J.*, *7*(3), 1079–1088, doi:10.2136/vzj2007.0115.

Javaux, M., V. Couvreur, J. Vander Borght, and H. Vereecken (2013), Root water uptake: From three-dimensional biophysical processes to macroscopic modeling approaches, *Vadose Zone J.*, *12*(4), doi:10.2136/vzj2013.02.0042.

Kalbacher, T., C. L. Schneider, W. Wang, A. Hildebrandt, S. Attinger, and O. Kolditz (2011), Modeling soil-coupled water uptake of multiple root system with automatic time stepping, *Vadose Zone J.*, *10*, 727–735, doi:10.2136/vzj2010.0099.

Kollet, S. J., and R. M. Maxwell (2006), Integrated surface–groundwater flow modeling: A free-surface overland flow boundary condition in a parallel groundwater flow model, *Adv. Water Resour.*, *29*(7), 945–958.

Kollet, S. J., and R. M. Maxwell (2008), Capturing the influence of groundwater dynamics on land surface processes using an integrated, distributed watershed model, *Water Resour. Res.*, *44*, W02402, doi:10.1029/2007WR006004.

Manoli, G., S. Bonetti, J.-C. Domec, M. Putti, G. Katul, and M. Marani (2014), Tree root systems competing for soil moisture in a 3D soil–plant model, *Adv. Water Resour.*, *66*, 32–42, doi:10.1016/j.advwatres.2014.01.006.

Maxwell, R. M., et al. (2014), Surface-subsurface model intercomparison: A first set of benchmark results to diagnose integrated hydrology and feedbacks, *Water Resour. Res.*, *50*, 1531–1549, doi:10.1002/2013WR013725.

Metselaar, K., and Q. De Jong Van Lier (2007), The shape of the transpiration reduction function under plant water stress, *Vadose Zone J.*, *6*(1), 124–139.

Moran, M. S., R. L. Scott, T. O. Keefer, W. E. Emmerich, M. Hernandez, G. S. Nearing, G. B. Paige, M. H. Cosh, and P. E. O'Neill (2009), Partitioning evapotranspiration in semiarid grassland and shrubland ecosystems using time series of soil surface temperature, *Agric. For. Meteorol.*, *149*(1), 59–72, doi:10.1016/j.agrformet.2008.07.004.

Morita, M., and B. C. Yen (2002), Modeling of conjunctive two-dimensional surface-three-dimensional subsurface flows, *J. Hydraul. Eng.*, *128*(2), 184–200, doi:10.1061/(ASCE)0733-9429(2002)128:2(184).

Niu, G.-Y., et al. (2014a), Incipient subsurface heterogeneity and its effect on overland flow generation—Insight from a modeling study of the first experiment at the Biosphere 2 Landscape Evolution Observatory, *Hydrol. Earth Syst. Sci.*, *18*(5), 1873–1883, doi:10.5194/hess-18–1873-2014.

Niu, G.-Y., C. Paniconi, P. A. Troch, R. L. Scott, M. Durcik, X. Zeng, T. Huxman, and D. C. Goodrich (2014b), An integrated modelling framework of catchment-scale ecohydrological processes: 1. Model description and tests over an energy-limited watershed, *Ecohydrology*, *7*(2), 427–439, doi:10.1002/eco.1362.

Orlandini, S., and R. Rosso (1998), Parameterization of stream channel geometry in the distributed modeling of catchment dynamics, *Water Resour. Res.*, *34*(8), 1971–1985.

Orlandini, S., G. Moretti, M. Franchini, B. Aldighieri, and B. Testa (2003), Path-based methods for the determination of nondispersive drainage directions in grid-based digital elevation models, *Water Resour. Res.*, *39*(6), 1144, doi:10.1029/2002WR001639.

Panday, S., and P. S. Huyakorn (2004), A fully coupled physically-based spatially-distributed model for evaluating surface/subsurface flow, *Adv. Water Resour.*, *27*, 361–382, doi:10.1016/j.advwatres.2004.02.016.

Paniconi, C., and M. Putti (1994), A comparison of Picard and Newton iteration in the numerical solution of multidimensional variably saturated flow problems, *Water Resour. Res.*, *30*(12), 3357–3374, doi:10.1029/94WR02046.

Pannell, D. J. (1997), Sensitivity analysis of normative economic models: Theoretical framework and practical strategies, *Agric. Econ.*, *16*, 139–152, doi:10.1016/S0169-5150(96)01217-0.

Reynolds, J. F., P. R. Kemp, and J. D. Tenhunen (2000), Effects of long-term rainfall variability on evapotranspiration and soil water distribution in the Chihuahuan desert: A modeling analysis, *Plant Ecol.*, *150*(1-2), 145–159, doi:10.1023/A:1026530522612.

Rigon, R., G. Bertoldi, and T. M. Over (2006), GEOtop: A distributed hydrological model with coupled water and energy budgets, *J. Hydrometeorol.*, *7*(3), 371–388, doi:10.1175/JHM497.1.

Sebben, M. L., A. D. Werner, J. E. Liggett, D. Partington, and C. T. Simmons (2013), On the testing of fully integrated surface–subsurface hydrological models, *Hydrol. Processes*, *27*, 1276–1285, doi:10.1002/hyp.9630.

Shen, C., and M. S. Phanikumar (2010), A process-based, distributed hydrologic model based on a large-scale method for surface–subsurface coupling, *Adv. Water Resour.*, *33*(12), 1524–1541, doi:10.1016/j.advwatres.2010.09.002.

Shen, C., J. Niu, and M. S. Phanikumar (2013), Evaluating controls on coupled hydrologic and vegetation dynamics in a humid continental climate watershed using a subsurface-land surface processes model, *Water Resour. Res.*, *49*, 2552–2572, doi:10.1002/wrcr.20189.

Šimůnek, J., and J. W. Hopmans (2009), Modeling compensated root water and nutrient uptake, *Ecol. Modell.*, *220*(4), 505–521, doi:10.1016/j.ecolmodel.2008.11.004.

Šimůnek, J., M. Šejna, H. Saito, M. Sakai, and M. T. van Genuchten (2013), *The HYDRUS-1D Software Package for Simulating the Movement of Water, Heat, and Multiple Solutes in Variably Saturated Media, HYDRUS Software Series 3*, version 4.16, pp. 340, Dep. of Environ. Sci., Univ. of Calif. Riverside, Riverside.

Skaggs, T., M. van Genuchten, P. Shouse, and J. Poss (2006), Macroscopic approaches to root water uptake as a function of water and salinity stress, *Agric. Water Manage.*, *86*(1-2), 140–149.

VandenBerg, A. H. M. (2009), Rock unit names in western Victoria, seamless geology project, *Tech. Rep. 130*, Geol. Surv. of Victoria, Melbourne, Victoria.

VanderKwaak, J. E., and K. Loague (2001), Hydrologic-response simulation for the R-5 catchment with a comprehensive phiscs-based model, *Water Resour. Res.*, *37*(4), 999–1013, doi:10.1029/2000WR900272.

van Genuchten, M. T. (1980), A closed-form equation for predicting the hydraulic conductivity of unsaturated soils, *Soil Sci. Soc. Am. J.*, *44*, 892–898.

Verma, P., S. P. Loheide II, D. Eamus, and E. Daly (2014), Root water compensation sustains transpiration rates in an Australian woodland, *Adv. Water Resour.*, *74*, 91–101, doi:10.1016/j.advwatres.2014.08.013.

Vivoni, E. R., J. C. Rodríguez, and C. J. Watts (2010), On the spatiotemporal variability of soil moisture and evapotranspiration in a mountainous basin within the North American monsoon region, *Water Resour. Res.*, *46*, W02509, doi:10.1029/2009WR008240.

Vrugt, J. A., M. T. vanWijk, J. W. Hopmans, and J. Šimůnek (2001), One-, two-, and three-dimensional root water uptake functions for transient modeling, *Water Resour. Res.*, *37*(10), 2457–2470, doi:10.1029/2000WR000027.

Wang, L., S. P. Good, and K. K. Caylor (2014), Global synthesis of vegetation control on evapotranspiration partitioning, *Geophys. Res. Lett.*, *41*, 6753–6757, doi:10.1002/2014GL061439.

Weill, S., E. Mouche, and J. Patin (2009), A generalized Richards equation for surface/subsurface flow modelling, *J. Hydrol.*, *366*, 9–20, doi:10.1016/j.jhydrol.2008.12.007.

Willmott, C. J. (1981), On the validation of models, *Phys. Geogr.*, *2*(2), 184–194.

Xiang, T., E. R. Vivoni, and D. J. Gochis (2014), Seasonal evolution of ecohydrological controls on land surface temperature over complex terrain, *Water Resour. Res.*, *50*, 3852–3874, doi:10.1002/2013WR014787.